Acta Cryst. (1987). B43, 258-265

An X-ray and Neutron Diffraction Study of $Cs_2Ti_5O_{11}$ and $Cs_2Ti_5O_{11}.X_2O$, X = H, D

BY JADWIGA KWIATKOWSKA

Institute of Nuclear Physics, ul. Radzikowskiego 152, 31 342 *Krakow, Poland*

IAN E. GREY AND IAN C. MADSEN

CSIRO Division of Mineral Chemistry, PO Box 124, *Port Melbourne, Victoria, Australia* 3207

AND LES A. BURSILL

School of Physics, University of Melbourne, Parkville, Victoria, Australia 3052

(*Received* 11 *June* 1986; *accepted* 22 *October* 1986)

Abstract

The structures of the new caesium titanate layer structures, $Cs_2Ti_5O_{11}$ and $Cs_2Ti_5O_{11}.X_2O$ (X = H, D), have been determined and refined using a combination of single-crystal and powder X-ray and powder neutron diffraction techniques. The anhydrous and hydrated oxides are both monoclinic, space group $C2/m$, $Z = 4$, with unit-cell parameters a = 19·718 (8), b = 3·808 (1), c = 15·023 (6) Å, β = 106·93 (3)°, V = 1079 Å^3, T = 523 K, and a = 23·849 (8), b = 3·800 (1), c = 14·918 (6) Å, β = 121·27 (3)°, V = 1156 Å^3, T = 297 K respectively. The final R values from Rietveld refinement of the powder neutron diffraction intensity data (2θ = 19–115°, λ = 1·893 Å) are: anhydrous phase, R_{wp} = 0·068, R_B = 0·017; hydrated phase, R_{wp} = 0·039, R_B = 0·011; and deuterated phase, R_{wp} = 0·072, R_B = 0·021. The structures comprise five-octahedra-wide ribbons of edge-shared, titanium-centred octahedra that link by corner sharing along [010] to give stepped (100) octahedral layers, separated by interlayer packing of Cs ions and H_2O. The interlayer ions are ordered in the hydrated phase but show only short-range order in the anhydrous phase. The hydration is accompanied by a sliding of the octahedral layers relative to one another along [001].

Introduction

We have recently reported the results of a phase study of the Cs_2O–TiO_2 system in the composition range 75–100 mole% TiO_2 and the temperature range 1123–1473 K (Grey, Madsen, Watts, Bursill & Kwiatkowska, 1985), which revealed the existence of two new caesium titanates at Ti/Cs atomic ratios near 3·0 and 2·5. The latter compound, $Cs_2Ti_5O_{11}$, was found to undergo a reversible hydration below 473 K to form $Cs_2Ti_5O_{11}.(1+x)H_2O$ ($0{\cdot}5 < x < 1$). It formed asbestos-like fibrous crystals, up to 1–2 mm length but only 1–5 μm in diameter. Crystals large enough for an X-ray diffraction (XRD) study were composed of aggregates of fibres in which individual fibres were slightly rotated relative to one another. The corresponding diffraction patterns (Weissenberg and precession) showed streaks and arcs in place of discrete spots, making the intensity data unsuitable for structure refinements. Consequently the structures were refined by the Rietveld method for both the anhydrous and hydrated phases using powder neutron and XRD data. In addition, a neutron powder refinement was carried out on a deuterated sample.

Experimental

The preparation of samples of the anhydrous and hydrated phases for XRD studies has been described previously (Grey *et al.*, 1985). For the neutron diffraction study, a 30 g mixture of $CsNO_3$ and TiO_2 was given a preliminary heat treatment in air at 1173 K for 16 h. The product was ground, pressed into 12 mm diameter pellets and heated for 16 h at 1273 K, then cooled to 573 K at 50 K h^{-1}.

To preserve the anhydrous form, some of the pellets were sealed in an aluminium can immediately after they were removed from the furnace. The remaining pellets were left in an open dish for 2 weeks to ensure complete hydration of the material.

The anhydrous specimen, after being used for the neutron diffraction (ND) experiment, was then deuterated. The aluminium can was opened in a nitrogen-filled glovebox and the specimen transferred onto a wire grating in a desiccator containing 200 ml of D_2O. The sample was left in the desiccator over D_2O for 2 weeks and then packed back into the aluminium can and sealed under nitrogen.

Oriented, needle-like aggregates of fibres were studied by the Weissenberg and precession methods. Diffraction patterns for the anhydrous phase were

0108-7681/87/030258-08$01.50

obtained while blowing hot helium gas (at ~473 K) onto the crystals, which were attached to glass fibres with silicone cement.

For the powder XRD studies on the hydrated phase, a sample was finely ground and side-mounted in an aluminium holder. Tests had shown that this was the most effective mounting technique for minimizing preferred orientation. Intensity measurements were made at 297 K at intervals of 0·04°, 2θ, using Cu Kα radiation and a step counting time of 5 s.The X-ray tube was operated at 45 kV and 30 mA, with 0·5° divergence and receiving slits for the 2θ range 7–23° and 1° slits for the 2θ range 17–80°. The two data sets were scaled using reflections in the common interval, 17–23°, and merged at 20°. These conditions allowed the collection of profile data for a total of 436 Bragg reflections with a maximum step intensity of 12 400 counts.

For the powder XRD studies on the anhydrous phase, the hydrated sample was side-mounted in a specially constructed circular sample holder fitted with a platinum resistance heater. The temperature was measured with an iron–constantan thermocouple embedded in the sample. Diffractograms were obtained at 20 K intervals between 323 and 523 K. Examples of some diffractograms obtained, together with the differential thermal analysis curve for the dehydration process are shown in Fig. 1. There was no change to the diffraction pattern associated with the first water-loss peaks below 403 K (Grey *et al.*, 1985). The main structural changes resulting from dehydration were associated with the strong, sharp endotherm at 443 K, and are reflected in the changes to the diffractograms illustrated in Fig. 1. The sample was held overnight at 523 K and then a step-scan intensity data set was obtained, using the conditions given above for the hydrated phase.

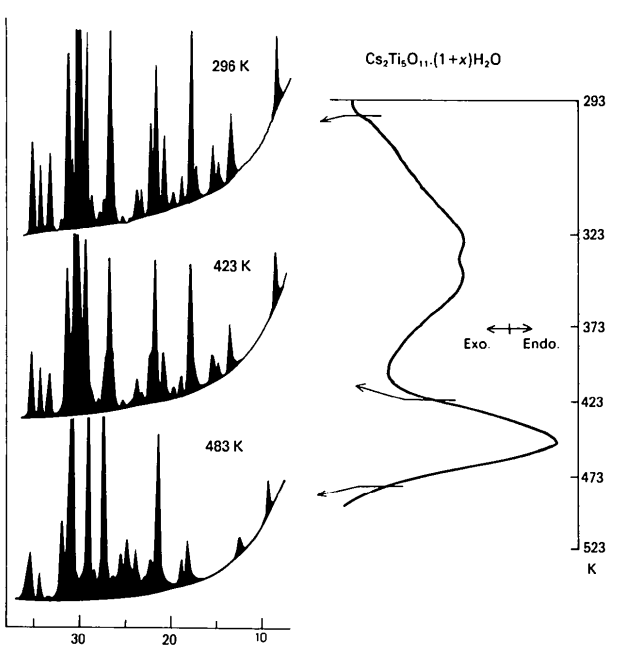

Fig. 1. Powder X-ray diffraction patterns for $Cs_2Ti_5O_{11}.H_2O$ at 296, 423 and 483 K showing the transformation from the hydrated to the anhydrous phase. The corresponding differential thermal analysis curve is shown on the right-hand side.

Neutron diffraction data were collected at 295 K on the high-resolution, fixed-wavelength, eight-counter diffractometer (HRPD) attached to the Australian Atomic Energy Commission HIFAR reactor at Lucas Heights, New South Wales. A single-counter version of this instrument has been described by Howard, Ball, Davis & Elcombe (1983). The specimen was contained in a 13×45 mm aluminium can and the data were collected in steps of 0·05° in the 2θ range 15–115°, at a wavelength of 1·893 Å. For the deuterated sample a step size of 0·04° was used.

Least-squares structure refinements of both the neutron and X-ray diffraction data sets were carried out with the Rietveld analysis program *DWB*3·2 (Wiles & Young, 1981) which has been extensively modified to include a 2θ-variable pseudo-Voigt peak-shape function (Hill & Howard, 1985) and a correction for absorption in the neutron beam (Hewat, 1979). The method of extraction of 'observed' integrated peak intensities for the calculation of Fourier coefficients and Bragg agreement indices has also been improved. The scattering lengths used for Cs, Ti, O, H and D were 5·42, −3·44, 5·80, −3·74 and 6·67 fm, respectively, while the neutral-atom X-ray scattering factors, including anomalous-dispersion corrections, were taken from *International Tables for X-ray Crystallography* (1974).

Structure determination and refinement

1. *Anhydrous phase*

An analysis of Weissenberg and precession photographs showed that the anhydrous phase had face-centred monoclinic symmetry, with possible space groups $C2/m$, Cm or $C2$, and with approximate unit-cell parameters, $a = 19{\cdot}7$, $b = 3{\cdot}8$, $c = 15{\cdot}0$ Å, $\beta = 107°$. The single-crystal data were used to index the XRD powder pattern obtained at 523 K (with α-Al_2O_3 as internal standard) and the 2θ values were used to refine the lattice parameters, giving the values listed in the *Abstract*.

A partial structure model was constructed for $Cs_2Ti_5O_{11}$, based on the observed similarity of its powder pattern to that of $Tl_2Ti_4O_9$ (Verbaere & Tournoux, 1973). The a, b and β parameters are almost the same for both compounds and c for $Cs_2Ti_5O_{11}$ is 3 Å longer than c for $Tl_2Ti_4O_9$ (corresponding to one octahedral edge). The latter compound has a structure based on four-octahedra-wide ribbons of edge-shared octahedra that corner-link along [010] to give stepped (100) octahedral layers,

with Tl^+ ions packing between the layers. On the basis that $Cs_2Ti_5O_{11}$ is the five-octahedra-wide structural homologue of the series $A_2Ti_nO_{2n+1}$, the titanium coordinates for the titanium-centred octahedral framework were derived from the geometry of the thallium titanate.

The calculated titanium coordinates were used in a refinement, in $C2/m$, of integrated X-ray powder peak intensities. These were obtained by application of the pattern deconvolution program *PROFIT* (H. Scott, 1985, private communication) to the X-ray powder profile data. The positions of the Cs and O atoms were obtained from Fourier and difference Fourier syntheses. When all atoms were located, the refinement was then continued using Rietveld analysis of the X-ray data. Refinement of the profile parameters included a scale factor; a pseudo-Voigt shape parameter (Hindeleh & Johnson, 1978); a 2θ zero parameter; a peak full width at half maximum (FWHM) function of the form $FWHM^2 = U\tan^2\theta + V\tan\theta + W$, where U, V and W are refineable parameters (Caglioti, Paoletti & Ricci, 1958); calculated for 3·5 half widths on either side of the peak maximum; a peak asymmetry parameter (Rietveld, 1969) for reflections with $d > 2{\cdot}2$ Å; and the unit-cell parameters. The background was evaluated by linear interpolation between 21 points uniformly distributed over the whole pattern. An experimentally determined value of 0·91 was used for the monochromator polarization correction (Hill & Madsen, 1984).

The refinements were initiated using group isotropic thermal vibration parameters $B(O) = 1$ and $B(M) = 0{\cdot}5$ Å^2. Refinement of metal-atom coordinates and Cs site occupation factors (partial occupancy of the Cs sites was established from Fourier analyses) converged at $R_{wp} = 0{\cdot}10$. Attempts to release the O coordinates in further refinements were unsuccessful, resulting in large oscillations of the coordinates. At this stage, neutron diffraction data were obtained and Rietveld refinement of the neutron data was commenced, using the coordinates obtained from the XRD analysis as a starting set. In contrast to the XRD profile, which had a large hump in the background, centred at $d = 3{\cdot}6$ Å (due to short-range order of the Cs atoms) the ND profile showed no significant background fluctuations and it was fitted by a five-parameter polynomial in $2\theta^n$, where n has values from 0 to 4 inclusive. Use of Fourier difference syntheses during the refinement showed elongated regions of high neutron-scattering density along [001] in the interlayer region, due to disorder of Cs atoms. This disorder was satisfactorily modelled using four partially occupied Cs sites. Refinement of profile parameters, all coordinates, site-occupation factors for Cs and group isotropic thermal vibration parameters for Cs, Ti and O resulted in convergence at the refinement indices listed in Table 1.

Table 1. *Refinement indices*

	$Cs_2Ti_5O_{11}$			$Cs_2Ti_5O_{11}.H_2O$			$Cs_2Ti_5O_{11}.D_2O$
	ND	XRD-1	XRD-2	ND	XRD-1	XRD-2	ND
R_{wp}	0·068	0·062	0·059	0·039	0·083	0·085	0·072
R_B	0·017	0·067	0·081	0·011	0·090	0·091	0·021
S	3·12	9·4	9·0	2·04	11·7	16·0	1·76

Using the refined O parameters from the ND Rietveld analysis, the Rietveld refinement of the XRD data was then continued. It was found that convergence could not be achieved until the disorder of the interlayer Cs atoms was adequately modelled. From trial refinements it was found that the best model for fitting the XRD data involved three partially occupied Cs sites with anisotropic thermal vibration parameters for each site.

With the Cs disorder modelled as above, satisfactory convergence was achieved with refinement of all coordinates, Cs population parameters and anisotropic thermal vibration parameters, and group thermal vibration parameters for O and Ti. Two independently collected XRD data sets were refined and the corresponding R_{wp}, R_B and goodness-of-fit values are listed in Table 1. The final coordinates and thermal vibration parameters for the ND and the two XRD Rietveld refinements are given in Table 2, and the observed, calculated and difference diffraction profiles for the ND data set are presented in Fig. 2.*

2. *Hydrated phase*

Weissenberg and precession photographs showed that the hydrated phase had the same face-centred monoclinic symmetry as for the anhydrous phase, with similar b and c parameters, but with an enlarged β and a longer a parameter. The single-crystal data were used to index the XRD powder pattern, and refinement of the peak 2θ values from the powder data gave the unit-cell parameters reported in the *Abstract.*

The three different structure determination procedures were carried out and each led to the same structural model. Firstly, a model for the distribution of the Ti atoms was established from the geometrical relationship between the unit cells for the anhydrous and hydrated phases. The Ti atom model was refined using integrated powder XRD intensities obtained from application of the pattern-deconvolution program *PROFIT* to the profile data, and the Cs and O coordinates were obtained from Fourier and difference Fourier maps.

* Lists of numerical values corresponding to the data in Figs. 2 and 3, X-ray step intensity data, and bond lengths and angles have been deposited with the British Library Document Supply Centre as Supplementary Publication No. SUP 43577 (27 pp.). Copies may be obtained through The Executive Secretary, International Union of Crystallography, 5 Abbey Square, Chester CH1 2HU, England.

Table 2. *Refined structure parameters for* $Cs_2Ti_5O_{11}$

	x			y	z		
	ND	XRD-1	XRD-2		ND	XRD-1	XRD-2
(*a*) Atom coordinates with e.s.d.'s in parentheses							
Cs(1)	0·423 (1)	0·4222 (3)	0·4233 (3)	0·0	0·916 (2)	0·9096 (4)	0·9109 (4)
Cs(2)	0·471 (2)	0·4698 (7)	0·4681 (7)	0·0	0·718 (3)	0·718 (2)	0·720 (1)
Cs(3)	0·429 (2)			0·0	0·828 (3)		
Cs(4)	0·491 (2)	0·4858 (6)	0·4836 (6)	0·0	0·600 (2)	0·599 (2)	0·594 (2)
Ti(1)	0·248 (1)	0·2507 (6)	0·2516 (6)	0·0	0·129 (2)	0·1331 (9)	0·1347 (8)
Ti(2)	0·220 (1)	0·2185 (5)	0·2166 (7)	0·0	0·334 (2)	0·333 (1)	0·332 (1)
Ti(3)	0·190 (2)	0·1884 (7)	0·1879 (6)	0·0	0·519 (2)	0·5110 (8)	0·5131 (8)
Ti(4)	0·159 (1)	0·1600 (8)	0·1602 (8)	0·0	0·691 (2)	0·6975 (8)	0·6984 (8)
Ti(5)	0·124 (1)	0·1283 (7)	0·1281 (6)	0·0	0·896 (2)	0·895 (1)	0·896 (1)
O(1)	0·1838 (6)	0·187 (2)	0·182 (2)	0·0	0·025 (1)	0·034 (3)	0·031 (3)
O(2)	0·3474 (7)	0·347 (2)	0·347 (2)	0·0	0·114 (1)	0·112 (2)	0·109 (3)
O(3)	0·1735 (8)	0·188 (2)	0·180 (2)	0·0	0·204 (1)	0·204 (2)	0·202 (2)
O(4)	0·3146 (8)	0·313 (2)	0·311 (2)	0·0	0·290 (1)	0·309 (2)	0·302 (2)
O(5)	0·1424 (9)	0·142 (2)	0·151 (2)	0·0	0·390 (1)	0·390 (3)	0·387 (3)
O(6)	0·2814 (8)	0·289 (2)	0·291 (2)	0·0	0·471 (1)	0·463 (3)	0·471 (3)
O(7)	0·1207 (8)	0·120 (2)	0·115 (2)	0·0	0·565 (1)	0·559 (2)	0·560 (2)
O(8)	0·2533 (8)	0·256 (2)	0·256 (2)	0·0	0·653 (1)	0·662 (3)	0·660 (3)
O(9)	0·0932 (7)	0·086 (2)	0·089 (2)	0·0	0·746 (1)	0·746 (3)	0·744 (3)
O(10)	0·2355 (6)	0·230 (2)	0·228 (2)	0·0	0·853 (1)	0·820 (3)	0·837 (3)
O(11)	0·0437 (6)	0·053 (2)	0·051 (2)	0·0	0·915 (1)	0·904 (3)	0·908 (3)
(*b*) Thermal vibration parameters and population parameters (*PP*)							
Cs(1) *PP**	0·36 (2)	0·450 (6)	0·437 (6)	Cs(2) *PP*	0·20 (2)	0·29 (1)	0·28 (1)
$\beta 11 \equiv B$	0·5 (2)	0·0017 (3)	0·0015 (3)	$\beta 11 \equiv B$	0·5 (2)	0·0045 (8)	0·0043 (8)
$\beta 22$		−0·029 (6)	−0·006 (8)	$\beta 22$		0·10 (2)	0·06 (2)
$\beta 33$		0·014 (1)	0·012 (1)	$\beta 33$		0·014 (3)	0·015 (3)
$\beta 13$		−0·0019 (4)	−0·0032 (3)	$\beta 13$		−0·009 (1)	−0·008 (1)
Cs(3) *PP*	0·14 (1)			Cs(4) *PP*	0·27 (1)	0·27 (1)	0·26 (1)
B	0·5 (2)			$\beta 11 \equiv B$	0·5 (2)	0·0015 (5)	0·0003 (4)
				$\beta 22$		0·002 (1)	0·01 (1)
				$\beta 33$		0·012 (2)	0·012 (2)
				$\beta 13$		−0·0056 (7)	−0·0052 (6)
Ti *B*	0·7 (2)	1·29 (1)	0·5 (1)	O_x *B*	0·6 (2)	0·4 (2)	0·3 (2)

* Full occupancy corresponds to $PP = 0·5$.

In the second approach, the integrated powder intensities (119 reflections, up to $\sin\theta/\lambda = 0·35$) were reduced to structure factors and used in the direct-method program *EEES* (Sheldrick, 1976). It was necessary to introduce an additional 74 unobserved reflections with minimum F values to generate sufficient quartet relationships for the program to run. When this was done, the solution with the highest reliability index had the same arrangement of Cs and Ti atoms as established above from geometrical considerations.

The third approach made use of the ($h0l$) Weissenberg intensity data. The intensities of 166 ($h0l$) reflections were visually estimated by reference to a calibrated scale and were used to generate a Patterson projection along **b**. The positions of the Cs and Ti atoms were determined from the Patterson vectors and the O atoms were located in difference Fourier maps. The same model was obtained as from the first two procedures. It consists of stepped octahedral layers as in the anhydrous phase, defined by five independent Ti atoms and eleven O atoms, all in special positions 4(i) of space group $C2/m$, separated by layers of Cs ions. In contrast with the anhydrous phase, the two independent Cs ions are fully ordered in the hydrated phase. In addition, an O atom corresponding to a water molecule, in the layer containing the Cs ions, was identified in a difference Fourier map.

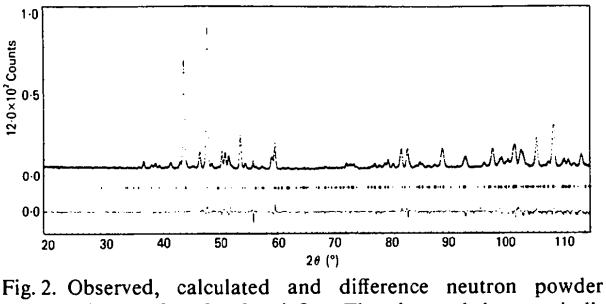

Fig. 2. Observed, calculated and difference neutron powder diffraction profiles for $Cs_2Ti_5O_{11}$. The observed data are indicated by points and the calculated profile is the continuous line overlaying them. The short vertical lines below the profile represent the positions of all possible Bragg reflections, and the bottom curve is the value of sign (Δ)$w\Delta^2$ at each step, where Δ is the difference between the observed and calculated intensity at each step in the profile.

The average atomic coordinates from the three structure determination procedures were used in a Rietveld refinement of the XRD powder profile intensity data. As with the anhydrous phase, only the metal-atom coordinates could be satisfactorily refined using the X-ray data, giving $R_{wp} = 0·12$. The refinement was then continued with the ND profile intensity data for the hydrated phase and convergence was achieved with refinement of the coordinates of all metals and octahedral layer O atoms. A difference Fourier map was generated to locate the atoms of the interlayer water molecule, but an unambiguous identification of the O and H atoms was not possible. This was considered to be due to some disorder in the position of the water molecule, resulting in partial

Table 3. *Refined structure parameters for* $Cs_2Ti_5O_{11}.X_2O$, X = H, D

	x				y	z			
	ND (X = D)	ND (X = H)	XRD-1	XRD-2		ND (X = D)	ND (X = H)	XRD-1	XRD-2
(a) Atom coordinates with e.s.d.'s in parentheses									
Cs(1)	0·414 (1)	0·413 (1)	0·4130 (3)	0·4123 (3)	0·0	−0·015 (2)	−0·010 (2)	−0·0192 (5)	−0·0200 (6)
Cs(2)	0·482 (1)	0·477 (1)	0·4822 (3)	0·4832 (3)	0·0	0·644 (2)	0·642 (2)	0·6453 (6)	0·6449 (6)
Ti(1)	0·247 (2)	0·251 (2)	0·2509 (7)	0·2519 (7)	0·0	0·142 (3)	0·133 (3)	0·140 (1)	0·142 (1)
Ti(2)	0·224 (2)	0·222 (2)	0·2233 (8)	0·2210 (9)	0·0	0·324 (3)	0·316 (3)	0·317 (1)	0·319 (1)
Ti(3)	0·191 (2)	0·182 (2)	0·1915 (8)	0·1918 (8)	0·0	0·481 (3)	0·478 (3)	0·491 (1)	0·489 (1)
Ti(4)	0·162 (2)	0·165 (2)	0·1615 (7)	0·1631 (8)	0·0	0·663 (3)	0·664 (3)	0·659 (1)	0·660 (1)
Ti(5)	0·139 (2)	0·138 (2)	0·1371 (7)	0·1388 (7)	0·0	0·834 (3)	0·844 (3)	0·844 (1)	0·848 (1)
O(1)	0·204 (1)	0·192 (1)	0·188 (2)	0·185 (2)	0·0	0·008 (2)	0·000 (2)	0·995 (4)	0·994 (4)
O(2)	0·334 (1)	0·337 (1)	0·344 (2)	0·333 (2)	0·0	0·141 (2)	0·145 (2)	0·158 (3)	0·153 (4)
O(3)	0·186 (1)	0·186 (1)	0·176 (2)	0·189 (2)	0·0	0·180 (2)	0·182 (2)	0·182 (4)	0·189 (4)
O(4)	0·310 (1)	0·315 (1)	0·313 (2)	0·315 (2)	0·0	0·318 (2)	0·324 (2)	0·310 (4)	0·314 (4)
O(5)	0·164 (1)	0·162 (1)	0·156 (2)	0·149 (2)	0.0	0·352 (2)	0·355 (2)	0·349 (4)	0·352 (4)
O(6)	0·293 (1)	0·280 (1)	0·281 (2)	0·300 (2)	0·0	0·496 (2)	0·483 (2)	0·493 (4)	0·496 (4)
O(7)	0·123 (1)	0·120 (1)	0·131 (2)	0·127 (3)	0·0	0·512 (2)	0·506 (2)	0·513 (2)	0·514 (4)
O(8)	0·250 (1)	0·254 (1)	0·256 (1)	0·259 (3)	0·0	0·652 (2)	0·646 (2)	0·649 (4)	0·642 (4)
O(9)	0·092 (1)	0·099 (1)	0·096 (3)	0·102 (2)	0·0	0·681 (2)	0·684 (2)	0·670 (3)	0·677 (4)
O(10)	0·227 (1)	0·226 (1)	0·224 (2)	0·218 (2)	0·0	0·826 (2)	0·829 (2)	0·824 (4)	0·823 (4)
O(11)	0·062 (1)	0·065 (1)	0·068 (2)	0·065 (2)	0·0	0·835 (2)	0·837 (2)	0·841 (4)	0·828 (5)
X(1)	0·079 (2)				0·0	0·204 (3)			
X(11)	0·118 (2)				0·0	0·291 (3)			
X(2)	0·012 (1)				0·0	0·159 (1)			
O(w)	0·045 (1)				0·0	0·129 (2)			
(b) Thermal vibration parameters and population parameters (PP)									
PP[Cs(1)]*	0·45 (2)	0·46 (2)	0·488 (7)	0·476 (7)					
PP[Cs(2)]	0·45 (2)	0·45 (2)	0·486 (4)	0·495 (5)					
B(Ti)	1·1 (7)	0·2 (2)	0·3 (2)	0·0 (2)					
B(O)	1·0 (4)	0·8 (7)	0·9 (3)	0·8 (3)					
B(D)	2·7 (6)	1·8 (7)	1·8	1·8					
β11 Cs(1)	2·1 (4)	2·1 (3)	0·0012 (3)	0·0012 (3)					
Cs(2)			0·0013 (3)	0·0021 (3)					
β22 Cs(1)			0·07 (1)	0·04 (1)					
Cs(2)			0·05 (1)	0·031 (9)					
β33 Cs(1)			0·0017 (8)	0·0024 (8)					
Cs(2)			0·005 (1)	0·000 (1)					
β13 Cs(1)			−0·0001 (4)	0·0001 (4)					
Cs(2)			−0·0027 (4)	−0·0021 (4)					

* Full occupancy for PP = 0·5.

overlap and annulment of the peaks due to O and H which have scattering lengths of opposite signs. Consequently a deuterated sample was prepared as described above and an ND intensity data set collected. Rietveld refinement of the profile data for the deuterated phase led directly to the location of the O and D positions in a difference Fourier map. One of the D atoms was split between two positions, each with half occupancy. With inclusion of the D and water O atoms, Rietveld refinement of all coordinates, group isotropic thermal vibration parameters and profile parameters resulted in convergence at values of the refinement indices in Table 1.

Using the water O and H coordinates from the deuterated-phase refinement, the hydrated-phase refinement was then continued with the ND intensity data until convergence was obtained, at values of the refinement indices given in Table 1. Refinement of the XRD profile data was also continued using the O coordinates obtained from the ND refinements as starting coordinates. Rietveld refinements were carried out for two independently collected XRD data sets and the final R_{wp}, R_B and goodness-of-fit values for the two refinements are given in Table 1. The refined structural parameters for the four data sets are given in Table 3. Observed, calculated and difference neutron difraction profiles are shown in

Fig. 3. Only one water molecule per $Cs_2Ti_5O_{11}$ was located from the structure refinement. Extra water, from DTA analyses (Grey *et al.*, 1985) is not structural and is either surface adsorbed or distributed randomly between the octahedral layers. Thus from the structure point of view, the composition of the hydrated phase is $Cs_2Ti_5O_{11}.H_2O$.

Discussion

For the hydrated phase, four independent data sets (two ND and two XRD) were refined and for the anhydrous phase, three separate data sets (one ND and two XRD) were studied. The grouping together of the coordinates from the different refinements in Tables 2 and 3 allows a comparison of the difference between the refined values relative to the Rietveld e.s.d.'s.

The refined O coordinates from the ND refinements have associated e.s.d.'s that are smaller by a factor of about two than those from the XRD refinements, whereas the reverse situation applies to the Cs and Ti coordinates. For the hydrated phase, an analysis has been carried out of the differences between the

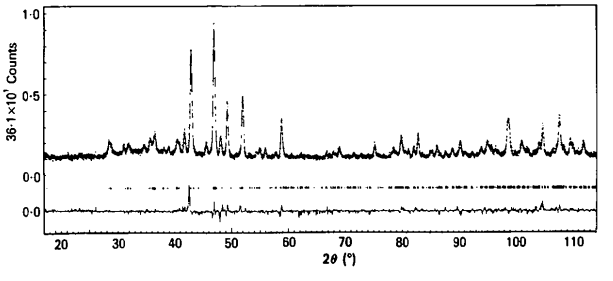

Fig. 3. Neutron powder diffraction profiles for $Cs_2Ti_5O_{11}.D_2O$. See Fig. 2 caption for definitions.

Table 4. *Analysis of coordinate variations for* $Cs_2Ti_5O_{11}.X_2O$

Data set pairs	Parameter variations as number of combined Rietveld e.s.d.'s: x Average	x >3 e.s.d.'s		z Average	z >3 e.s.d.'s	
N(1)–N(2)*	1·8 (1·6)†	O(1)	5·9	1·2 (0·7)	O(1)	3·3
		O(5)	3·5			
		O(6)	5·2			
X(1)–X(2)	1·4 (1·1)	O(1)	4·7	0·7 (0·5)		
		O(8)	3·2			
N(1)–X(1)	1·8 (1·5)	O(1)	4·0	1·3 (1·0)	O(2)	3·4
		O(6)	5·3			
		O(8)	3·3			
N(1)–X(2)	1·8 (1·7)	O(5)	3·3	1·4 (0·9)	Cs(1)	3·8
		O(6)	6·3			
		O(9)	5·0			
N(2)–X(1)	1·5 (1·4)	Cs(2)	4·0	1·4 (1·1)	Cs(1)	3·7
		Ti(3)	3·4	Ti(3)	3·2	
		O(7)	3·7			
		O(8)	3·3			
N(2)–X(2)	1·8 (1·9)	Cs(2)	4·8	1·4 (0·9)	Cs(1)	3·8
		Ti(3)	3·5			
		O(1)	6·7			
		O(9)	4·3			

* N(1) = ND (X = D); N(2) = ND (X = H).

† Numbers in parentheses are e.s.d.'s for average parameter variations over all coordinates.

coordinates in the four data sets, treated in pairs, and the results are presented in Table 4 in terms of the number of combined Rietveld e.s.d.'s that pairs of coordinates differ by. The results are given for the average of all coordinate differences for each pair of data sets as well as the individual differences that are greater than three combined Rietveld e.s.d.'s. There is no significant difference in the average deviations between coordinates associated with the pairs of ND sets as compared with those from the pairs of XRD sets and the four ND-XRD combinations. The average difference between pairs of equivalent coordinates over all data sets is 1·7 (1·5) and 1·2 (0·9) combined Rietveld e.s.d.'s for x and z respectively. Those deviations greater than three combined e.s.d.'s are individually listed in Table 4. They are reasonably uniformly distributed over all six pair combinations. The largest deviations are associated with the x coordinate for atoms O(1) and O(6). As can be seen from Table 3, the coordinates for these two atoms are related by a pseudo-face-centering relationship in the *ac* plane and so they do not contribute to reflections with $(h+l)$ odd. In the indexed XRD powder pattern for the hydrated phase (Table II, Grey *et al.*, 1985), it is seen that nine of the first twelve reflections have $h+l=2n+1$ and thus their intensities will be insensitive to O(1) and O(6). A similar pseudo-face-centering occurs for the O pairs O(8), O(10) and O(2), O(9), and as shown in Table 4, large coordinate deviations are associated with O(8) and O(9). This supports the well-known observation that caution should be exercised when analysing structural parameters from refined structures containing pseudosymmetry-related atom subgroups.

The structures of the anhydrous and hydrated phases are shown in projection along **b** in Figs. 4 and 5 respectively. They both comprise five-octahedra-wide ribbons of lepidocrocite-like groupings of edge-shared octahedra that are linked together by corner sharing to form (100) stepped-layers. The octahedral layers alternate with layers of Cs ions (and water molecules in the case of the hydrated phase). A comparison of Figs. 4 and 5 shows that the reversible hydration/dehydration reaction is accompanied by a sliding of the octahedral layers relative to one another to increase/decrease the interlayer volume in the vicinity of the corner-shared octahedral steps. The displacement of the layers is parallel to the edge-shared strings of five octahedra in the lepidocrocite-type ribbons and has a magnitude of about 1·5 octahedral edges (4·5 Å).

Dehydration is accompanied by a loss of long-range ordering of the Cs ions as shown by the partially occupied Cs sites in Table 2 and Fig. 4. An electron diffraction study of the anhydrous phase showed diffuse superlattice reflections resulting from short-range ordering of the Cs ions (Grey *et al.*, 1985; Kwiatkowska, 1985). The superlattice reflections were in the form of diffuse streaks along **a***. The intersection of the streaks with the b^*c^* plane gave relatively sharp spots, requiring a doubling of both the b and c parameters to index them. The Cs ordering is thus reasonably well developed within individual (100) planes, but there is little correlation between the

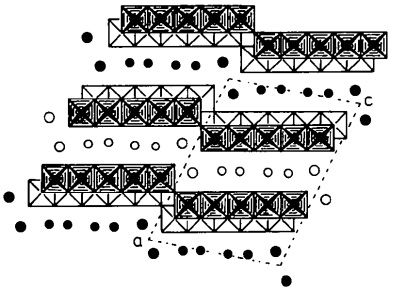

Fig. 4. Polyhedral representation of the structure of $Cs_2Ti_5O_{11}$ viewed along **b**. The open and filled circles represent partially occupied Cs sites at $y=0$ and $y=\frac{1}{2}$ respectively, as determined from the XRD refinement. Areas of circles are proportional to occupancies.

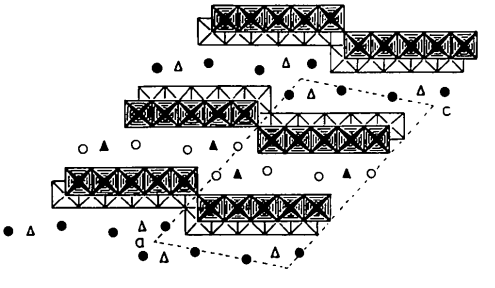

Fig. 5. Polyhedral representation of the structure for $Cs_2Ti_5O_{11}.X_2O$, viewed along **b**. The open circles and triangles represent Cs and X_2O respectively at $y=0$ and the filled symbols correspond to atoms at $y=\frac{1}{2}$.

Table 5. *Selected interatomic distances* (Å) *for* $Cs_2Ti_5O_{11}$

Ti(1)–O(1)		1·71 (2)	Ti(2)–O(3)		1·90 (3)
–O(10)	(×2)	1·98 (7)	–O(5)		1·95 (2)
–O(2)		2·04 (3)	–O(8)	(×2)	1·970 (7)
–O(3)		2·09 (3)	–O(6)		2·07 (3)
–O(4)		2·38 (3)	–O(4)		2·15 (3)
Ti(3)–O(7)		1·70 (4)	Ti(4)–O(9)		1·73 (3)
–O(5)		1·89 (3)	–O(7)		1·81 (3)
–O(6)	(×2)	1·98 (1)	–O(4)	(×2)	1·974 (7)
–O(8)		2·03 (3)	–O(8)		2·10 (3)
–O(6)′		2·13 (4)	–O(10)		2·25 (3)
Ti(5)–O(11)		1·68 (3)	Cs(1)–O(3)	(×2)	2·91 (2)
–O(1)		1·94 (2)	–O(11)	(×2)	3·05 (2)
–O(2)	(×2)	2·01 (1)	–O(11)′	(×2)	3·10 (2)
–O(9)		2·16 (3)	–O(1)	(×2)	3·16 (2)
–O(10)		2·63 (3)	–O(10)		3·54 (2)
			–O(2)		3·70 (3)
Cs(3)–O(3)	(×2)	2·72 (3)	Cs(4)–O(9)	(×2)	3·15 (2)
–O(11)	(×2)	2·95 (3)	–O(5)	(×2)	3·29 (3)
–O(8)		3·70(4)	–O(7)	(×2)	3·34 (3)
–O(5)	(×2)	3·70 (4)	–O(7)′	(×2)	3·39 (3)
–O(10)		3·85 (8)	–O(4)		3·70 (3)
Cs(2)–O(9)	(×2)	3·01 (3)			
–O(5)	(×2)	3·02 (3)			
–O(11)	(×2)	3·45 (3)			
–O(2)		3·74 (3)			
–O(3)	(×2)	3·87 (4)			

Table 6. *Selected interatomic distances* (Å) *for* $Cs_2Ti_5O_{11}.X_2O$, X = H, D

		H	D			H	D
Ti(1)–O(1)		1·74 (4)	1·70 (4)	Ti(2)–O(3)		1·71 (5)	1·70 (6)
–O(2)		1·95 (5)	2·07 (6)	–O(5)		1·79 (6)	1·84 (5)
–O(10)	(×2)	1·98 (1)	1·98 (1)	–O(8)	(×2)	1·98 (1)	1·97 (1)
–O(3)		2·03 (6)	1·81 (6)	–O(6)		2·13(5)	2·22 (4)
–O(4)		2·43 (4)	2·25 (4)	–O(4)		2·16(6)	2·08 (6)
Ti(3)–O(5)		1·65 (5)	1·68 (5)	Ti(4)–O(9)		1·75 (6)	1·82 (6)
–O(7)		1·72 (6)	1·93 (6)	–O(7)		2·02 (5)	1·94 (5)
–O(6)	(×2)	2·06 (1)	1·93 (1)	–O(4)	(×2)	1·95 (1)	1·99 (1)
–O(8)		2·18 (4)	2·18 (4)	–O(10)		2·11(4)	2·09 (4)
–O(6)′		2·30 (6)	2·30 (5)	–O(8)		2·27 (6)	2·19 (5)
Ti(5)–O(11)		1·69 (5)	1·84 (5)	Cs(1)–O(11)	(×2)	3·03 (3)	3·09 (3)
–O(2)	(×2)	1·97(1)	1·98 (1)	–O(3)	(×2)	3·08 (2)	3·05 (2)
–O(1)		1·99 (4)	2·23 (4)	–O(1)	(×2)	3·20 (3)	3·46(3)
–O(9)		2·05 (5)	1·95 (4)	–O(w)	(×2)	3·21 (4)	3·02 (3)
–O(10)		2·22 (6)	2·16 (5)	–O(w)′	(×2)	3·31 (7)	3·31 (2)
				–O(2)		3·61 (5)	3·71 (4)
				–O(10)		3·81 (3)	3·83 (3)
O(w)–X(1)			0·99 (4)	Cs(2)–O(7)	(×2)	2·92 (2)	3·04 (2)
–X(2)			1·09 (4)	–O(11)	(×2)	3·18 (3)	3·11 (2)
O(5)–X(11)			0·99 (4)	–O(9)	(×2)	3·25 (3)	3·04 (3)
X(1)–X(2)			1·37 (4)	–O(5)	(×2)	3·84 (4)	3·99 (4)
X(1)–O(5)			2·07 (4)	–O(2)		3·90 (3)	3·86 (3)
X(2)–O(11)			1·82 (4)	–O(w)	(×2)	3·98 (8)	>4
X(11)–O(w)			2·13 (4)				

ordering in successive layers. Models for the ordering of Cs ions within the (100) layers have been developed and they reproduce the intensity distribution of the superlattice reflections in the electron diffraction patterns (Kwaitkowska, 1985). In the powder patterns, the superlattice streaks appear as broad humps, *e.g.* as shown at $2\theta = 25°$ in the XRD pattern in Fig. 1. In the Rietveld analysis these humps were treated as part of the background and so only the average Cs-ion ordering was established as shown in Fig. 4. Hydration of the anhydrous phase leads to long-range ordering of Cs ions and water molecules as shown in Fig. 5. This ordering takes place, albeit slowly, even when the anhydrous phase is cooled from the preparation temperature in a moisture-free environment and then exposed to H_2O/D_2O at ambient temperature (as shown by the refinement of the deuterated phase which was prepared in this way).

Ti–O and Cs–O bond lengths for the anhydrous phase are given in Table 5 and those for the hydrated and deuterated phases are compared in Table 6. A more complete set, including O–O and Ti–Ti bonds, as well as O–Ti–O angles, has been deposited.* The bond lengths were all calculated using the coordinates derived from the ND Rietveld refinements, because of the greater reliability of the ND-derived O coordinates. The atom labelling for Ti and O in Tables 5 and 6 corresponds to equivalent locations in the octahedral framework for the anhydrous and hydrated phases, as shown for the latter phase in Fig. 6.

In each of the structures, the Ti-centred octahedra are highly distorted, with one or two very short Ti–O bonds, *ca* 1·7 Å, and at least one long Ti–O bond, 2·1–2·6 Å. The Ti-atom displacements from the centres of the octahedra are illustrated for the hydrated/deuterated phase in Fig. 6, which is a (010) slice through the structure at $y = 0$. The Ti displacements represent an attempt by the structure to balance local variations in the electrostatic valence sums at the different O sites. In the lepidocrocite-like segments, two types of anion sites occur; the inner equatorial/apical anions of the octahedra (which form the troughs in the corrugated layers) are shared between four cations, whereas the outer-equatorial anions (along the ridges of the corrugated layers) are shared between only two cations. In lepidocrocite itself, $Fe^{3+}OOH$, these two anion sites are occupied by O and a hydroxyl group respectively and local electroneutrality is achieved. However in the titanate layer structures the composition within the lepidocrocite-like ribbons is $Ti^{4+}O_2$ and so the apical O atoms, O(4), O(6), O(8) and O(10), are severely oversaturated whereas the outer equatorial O atoms, O(3),

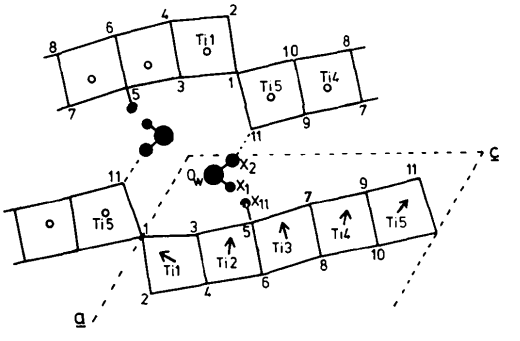

Fig. 6. Partial representation of the structure of $Cs_2Ti_5O_{11}.X_2O$, showing atoms in the vicinity of the X_2O molecule at $y = 0$. Displacements of the Ti atoms from the centres of the octahedra are shown (exaggerated).

* See deposition footnote.

O(5), O(7) and O(9), are undersaturated. To relieve this electrostatic imbalance, the Ti atoms are displaced towards the outer octahedral edges. Further charge compensation is achieved *via* bonds of the outer equatorial O atoms to Cs ions.

A large local charge imbalance also occurs where the octahedral ribbons join together by corner sharing. For example the corner-linked O(1) is shared between two Ti atoms and the outer-equatorial O(11) is bonded to only one Ti atom. The large displacements of the Ti atoms towards these undersaturated O atoms are illustrated in Fig. 6. In the case of the anhydrous phase, the attempts to balance the severe undersaturation of O(11) by displacement of Ti(5) results in an essentially five-coordinated site, with a very long sixth bond to O(1) of 2·63 (3) Å. Similar large distortions, with a tendency towards five-coordinate Ti have been previously noted in the related compound $Tl_2Ti_4O_9$ (Verbaere & Tournoux, 1973).

For the anhydrous phase the Cs site with highest occupancy, Cs(1) has a distorted cubic coordination, with Cs(1)–O bond lengths in the range 2·91 (2)–3·16 (2) Å. The cube is capped on two sides with longer bonds to O(10) and O(2) of 3·54 (2) and 3·70 (3) Å respectively. The nearest-neighbour (Cs–O < 3·5 Å) coordination of the minor Cs(2) and Cs(4) is trigonal-prismatic and cubic, respectively, with three and one additional longer bonds (3·7–3·9 Å), respectively. The identity of the minor site Cs(3) is doubtful, because as discussed above a better refinement of the XRD data was achieved with this site empty and with anisotropic thermal vibration parameters for the other Cs atoms.

In the hydrated and deuterated samples, Cs(1) has distorted pentagonal prismatic coordination, with six bonds to the framework O(1), O(3) and O(11) atoms and four bonds to the interlayer water molecules. The prism is capped on two faces by longer bonds to O(2) and O(10). The second Cs site, Cs(2), has distorted trigonal prismatic coordination, with pairs of bonds to O(9), O(7) and O(11), all less than 3·3 Å. The next nearest O atoms are over 3·8 Å away.

The geometry of the interlayer water molecule, as determined from the Rietveld refinement for the ND deuterated sample, shows a splitting of one of the proton sites. This is illustrated in Fig. 6. The fully occupied site $X(2)$ (X = H, D) forms a hydrogen bond to the framework O(11) atom. The split site is distributed equally between $X(1)$ which is bonded to O(w) and $X(11)$ which is directly bonded to the octahedral layer O atom, O(5). The distances O(w)–$X(1)$, O(w)–$X(2)$ and O(5)–$X(11)$ are in the range 0·99–1·09 Å and correspond to normal O–X distances, although the angle $X(1)$–O(w)–$X(2)$ is considerably smaller, 83(4)°, than is usual for a water molecule. The results suggest that an equilibrium exists of the type:

$$H_2O + O^{2-} \rightleftarrows (OH)^-_{\text{framework}} + (OH)^-_{\text{free}}$$

i.e. the water molecule transfers a proton to the framework O(5) atom to give an interlayer hydroxyl and a framework hydroxyl. The presence of both water and hydroxyls was detected in the infrared spectrum of the hydrated phase (Grey *et al.*, 1985). (The infrared study also showed the presence of H_3O^+, which presumably replaces Cs^+ since the refined Cs site occupancies were less than one, Table 3.)

The bonding of a proton to the O(5) site is consistent with local charge balance requirements, since O(5) is the only outer-equatorial O (*i.e.* with bonds to only two Ti atoms) that has no significant bonds to Cs ions. Whereas the outer-equatorial O atoms, O(1), O(3), O(7), O(9) and O(11) all have pairs of bonds to Cs ions in the range 3·04–3·46 Å, the O(5)–Cs shortest distance is essentially non-bonding at 3·99 (4) Å.

The presence of the unusual water–hydroxyl equilibrium warrants further study, *e.g.* using inelastic neutron scattering to determine if it is dynamic or static, as well as studies on the ion-exchange properties of the hydrated phase.

We thank Dr H. Scott for obtaining integrated X-ray powder intensities, by application of his pattern decomposition program, *PROFIT*, Mr J. A. Watts for his contributions to the single-crystal studies, and Ms C. Li for help with the powder preparations.

References

CAGLIOTI, G., PAOLETTI, A. & RICCI, F. P. (1958). *Nucl. Instrum.* **3**, 223–228.

GREY, I. E., MADSEN, I. C., WATTS, J. A., BURSILL, L. A. & KWIATKOWSKA, J. (1985). *J. Solid State Chem.* **58**, 350–356.

HEWAT, A. W. (1979). *Acta Cryst.* A**35**, 248.

HILL, R. J. & HOWARD, C. J. (1985). *J. Appl. Cryst.* **18**, 173–180.

HILL, R. J. & MADSEN, I. C. (1984). *J. Electrochem. Soc.* **131**, 1486–1491.

HINDELEH, A. M. & JOHNSON, D. J. (1978). *Polymer*, **19**, 27–32.

HOWARD, C. J., BALL, C. J., DAVIS, R. L. & ELCOMBE, M. M. (1983). *Aust. J. Phys.* **36**, 507–518.

International Tables for X-ray Crystallography (1974). Vol. IV. Birmingham: Kynoch Press. (Present distributor D. Reidel, Dordrecht.)

KWIATKOWSKA, J. (1985). PhD Thesis, Melbourne Univ., Physics Department.

RIETVELD, H. M. (1969). *J. Appl. Cryst.* **2**, 65–71.

SHELDRICK, G. M. (1976). *SHELX*76. Program for crystal structure determination. Univ. of Cambridge.

VERBAERE, A. & TOURNOUX, M. (1973). *Bull. Soc. Chim. Fr.* **4**, 1237–1241.

WILES, D. B. & YOUNG, R. A. (1981). *J. Appl. Cryst.* **14**, 149–151.